



Thomas algorithm; however, these algorithms are inherently sequential, with each block dependent on the preceding one in a chain-like manner. Moreover, even when each block can be of substantial size, the individual BLAS/LAPACK operations on a single block may be overshadowed by kernel launch overhead, and the size of each block may not be sufficient to fully utilize the computational resources of a modern GPU. As a result, a serial call to a large number of small BLAS/LAPACK operations leads to significant kernel launch overheads and underutilization of the GPU’s computational resources, making naive GPU implementations that simply iterate through the blocks unable to achieve high performance.

To address this limitation, this paper presents a recursive Schur complement-based strategy, a technique also known as *substructuring* in the domain decomposition literature [23, 25] (described in Figure 1.1). Similar formulations have been explored in the context of block-tridiagonal systems [5], but without exploiting batched BLAS/LAPACK kernels, which are the central focus of our work. In particular, a symmetric permutation is employed to reorganize the matrix into a substantial set of independent interior blocks, along with a smaller set of coupling separator variables. This reordering facilitates the computationally intensive elimination of all interior segments, allowing it to be executed in a single, massively parallel stage using batched kernels. The resulting smaller, denser, and still block-tridiagonal Schur complement system focuses solely on the separators, which are then solved by recursively applying the same procedure. This recursive approach systematically transforms a sparse, latency-bound problem into a hierarchy of dense, compute-bound kernels that are well-suited for GPU execution. Furthermore, given that the block-tridiagonal structure is known a priori, we can perform *tailored* reordering that leverages this structure, thereby enhancing GPU utilization. We will later present a tailored recursive partitioning strategy that can maximize the utilization of parallel computing capabilities and achieve favorable scaling results for parallel execution.

The proposed strategy specifically aims to leverage batched basic linear algebra subprograms (BLAS)/linear algebra package (LAPACK) in an optimized manner. Batched variants of BLAS and LAPACK routines hold significant promise for accelerating the solution of these systems, as demonstrated in [21]. These operations perform identical linear algebra operations across a large number of independent small to medium-sized matrices, effectively eliminating kernel launch overhead and maximizing GPU utilization. The recursive Schur-complement-based strategy

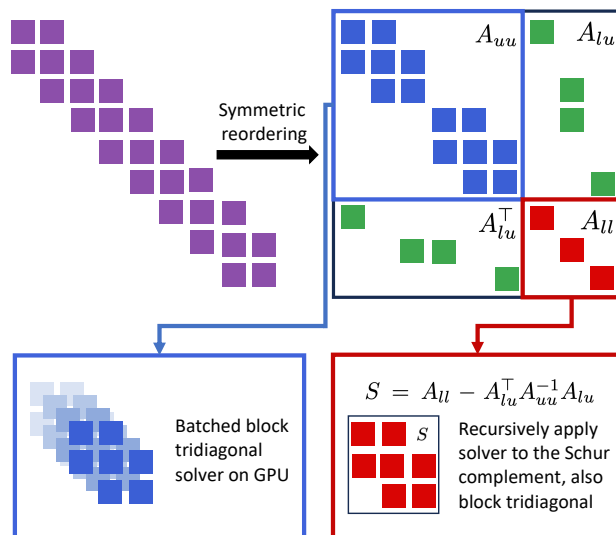


Figure 1.1: An overview of recursive Schur complement strategy for factorizing and solving block-tridiagonal systems.

described above can be implemented using three standard batched BLAS/LAPACK routines: Cholesky factorization (`potrf`), triangular solve (`trsm`), and matrix-matrix multiplication (`gemm`), all of which are widely available in vendor-specific or open-source GPU libraries. All these kernels rely on multiply-accumulate operations at their core, making them particularly well-suited to exploit the high computational throughput of modern GPUs, including tensor cores. Furthermore, since we target SPD systems, numerical pivoting techniques typically used in `getrf` or `sytrf` kernels—which can potentially slow down computation—are unnecessary. Thus, the factorization phase remains highly parallelizable and efficient.

The recursive Schur complement strategy described above is implemented in our open-source solver, **TBD-GPU**. The solver takes in the block-tridiagonal components as inputs and offers numerical factorization and solve capabilities (with support for multiple right-hand sides). Leveraging the multiple dispatch feature [6], our solver is designed to seamlessly switch between CUDA and ROCm backends while also supporting both single and double precision floating-point arithmetic.

### 1.1 Related Work

*Classical and Parallel Tridiagonal Algorithms.* The Thomas algorithm is a serial algorithm for solving tridiagonal systems [26] (i.e.,  $n = 1$  in (1.1)) with  $O(N)$  time complexity. To overcome this bottleneck, parallel algorithms such as cyclic reduction (CR) [11] and block cyclic reduction [24] were developed. While these

methods expose significant parallelism, it often comes at the cost of increased arithmetic operations or reduced numerical stability. A comprehensive survey of these methods is provided by Gander and Golub [10]. Block-tridiagonal extensions of these algorithms are critical in domains like Kalman smoothing and optimal control, where block sizes may be small but the problem horizon  $N$  is large. Although stable block elimination approaches are well established [4], developing efficient and robust formulations for massively parallel architectures remains an active area of research. Note that block variants of the Thomas algorithms and cyclic reduction methods are special cases of the recursive Schur complement framework presented in this paper. Our Schur complement method allows for a trade-off between arithmetic complexity and enhanced parallelism and GPU utilization.

*GPU Math Libraries and Batched Kernels.* The implementation of GPU solvers can largely benefit from vendor-provided dense linear algebra libraries. NVIDIA provides cuBLAS for dense operations, cuSOLVER for factorizations, and cuSPARSE/cuDSS for sparse direct methods [15, 17, 18, 16]. AMD offers similar functionality through its ROCm ecosystem [1]. The routines available in these libraries are highly optimized at the hardware architecture level, and thus, enables high-performance linear algebra operations. The key enabler for solving many small to medium-sized structured problems is the emergence of *batched* BLAS and LAPACK kernels. These routines amortize kernel launch overhead and maintain high GPU utilization by executing the same operation across thousands of independent matrices. This is ideal for problems that are too small to individually saturate the hardware. The Batched BLAS (BBLAS) interface proposal [8], along with implementations in MAGMA [28] and vendor libraries, has made these powerful primitives widely accessible. Our algorithm leverages these batched kernels to maximize high-throughput operations during block eliminations.

*Block-Tridiagonal Solvers on GPU.* Several libraries specifically target tridiagonal or block-tridiagonal systems on GPUs. TridiGPU offers bandwidth-optimized implementations of the Thomas algorithm and PCR variants [13], while PaScaL-TDMA implements a hybrid Thomas/PCR approach for CUDA [12]. The PfSolve framework generalizes cyclic reduction strategies across multiple architectures, including GPUs [27]. AMD’s ROCm library contains a block-tridiagonal factorization routines [1], but as of this writing (ROCm v6.4.1), this routine currently do not work for all problem sizes. These solvers achieve excellent performance for scalar tridiagonal or narrow-banded systems, but they generally do not leverage the

modern GPU architecture like tensorcores and support the large block sizes or hierarchical Schur complement factorizations required for handling a large number of blocks. Our work addresses this gap by combining stable block elimination with recursive batching and GPU-optimized kernels.

**1.2 Contributions** This paper presents two primary contributions:

*First, we introduce a recursive Schur-complement strategy optimized for block-tridiagonal systems, focusing on leveraging batched BLAS/LAPACK operations on GPUs.* While nested Schur complement strategies have been explored in the literature [29], their application has been confined mainly to dynamic programming contexts and has yet to be studied in relation to SPD block-tridiagonal systems. Furthermore, the algorithm has not been contextualized within the framework of batched BLAS/LAPACK operations. Although the use of batched BLAS/LAPACK operations in general sparse direct solvers has been investigated previously [21], our work specifically tailors the algorithm to the block-tridiagonal structure, enabling the implementation of optimized reordering strategies that enhance maximal GPU utilization.

*Second, we present a GPU implementation of the proposed algorithm, **TBD-GPU**<sup>1</sup>, which is open-source and cross-platform, providing support for both NVIDIA and AMD GPUs through CUDA and ROCm backends, respectively. This facilitates a *comprehensive performance analysis* of our implementation and allows us to compare it against other existing GPU and CPU solvers. With this implementation, we demonstrate the practical advantages gained from the optimized utilization of batched BLAS/LAPACK routines.*

**1.3 Paper outline.** The remainder of this paper is organized as follows. In Section 2, we formalize the block-tridiagonal problem and detail the standard sequential elimination algorithm. We analyze its computational complexity and discuss its limitations concerning parallelism. In Section 3, we introduce a recursive Schur-complement-based parallel algorithm for block-tridiagonal systems. This section outlines the specifics of our approach, including matrix reordering and partitioning strategies, batched GPU kernels, and the phases of recursive factorization and solution. We also examine methods for performing tailored reordering to maximize GPU utilization. Implementation details and numerical experiments are presented in Section 4, followed by concluding remarks in Section 5.

<sup>1</sup><https://anonymous.4open.science/r/TBD-GPU>

**2 Sequential Algorithm** In this section, we introduce a sequential algorithm for factorizing and solving SPD block-tridiagonal systems. This method is self-contained but also serves as a building block for our parallel recursive algorithm presented in Section 3. The serial method described here consists of a two-stage process: a numerical factorization followed by a block triangular solve. This approach is a specialized form of block Gaussian elimination that efficiently computes the factors required to solve the system.

**2.1 Factorization** The sequential factorization is essentially a block variant of the standard Cholesky factorization procedure,  $A = LL^T$ , where

$$L = \begin{bmatrix} L_{1,1} & & & & \\ L_{2,1} & L_{2,2} & & & \\ & & \ddots & \ddots & \\ & & & L_{N,N-1} & L_{N,N} \end{bmatrix},$$

as detailed in Algorithm 2.1. In each step of this process, the upper Cholesky factor  $L_{j,j}$  of each (modified) diagonal block  $A_{j,j}$  is computed first. Subsequently, the `trsm` operation is applied to obtain an off-diagonal factor  $L_{j,j+1}$ . Finally, the `gemm` operation performs a rank- $n$  update to form the Schur complement for the next diagonal block  $A_{j+1,j+1}$ , effectively eliminating the sub-diagonal entry for the current block. Note that in Algorithm 2.1, the `potrf` operations are conducted in place, so we do not introduce a separate array to store  $L$ .

---

**Algorithm 2.1** Serial Block-Cholesky Factorization

---

**Require:** Block tri-diagonal matrix  $A$ ; Number of diagonal blocks  $J$ .

- 1:  $A_{11} \leftarrow \text{cholesky}(A_{11})$  ▷ `potrf`
  - 2: **for**  $j = 1$  to  $J - 1$  **do**
  - 3:  $A_{j+1,j}^\top \leftarrow A_{j,j}^{-1} A_{j,j+1}$  ▷ `trsm`
  - 4:  $A_{j+1,j+1} \leftarrow A_{j+1,j+1} - A_{j+1,j} A_{j+1,j}^\top$  ▷ `gemm`
  - 5:  $A_{j+1,j+1} \leftarrow \text{cholesky}(A_{j+1,j+1})$  ▷ `potrf`
  - 6: **end for**
- 

**2.2 Triangular Solve** Once the factorization is complete, the  $A$  factor can be reused to solve the system for any given number of right-hand side vectors. The solve process, illustrated in Algorithm 2.2, involves two passes. A forward substitution pass computes an intermediate solution  $Y$ , followed by a backward substitution pass that determines the final solution  $X$ . Each step in these passes involves a block matrix-matrix product (`gemm`) and a triangular solve (`trsm`).

**2.3 Computational Complexity and Limitations** The factorization exhibits a time complexity of  $\mathcal{O}(Nn^3)$ , and the solve stage has a complexity of

---

**Algorithm 2.2** Serial Block-Cholesky Solve

---

**Require:** Factor  $A$ ; RHS  $B$ .

**Ensure:** Solution  $X$ .

- 1: – *Forward substitution* –
  - 2:  $Y_1 \leftarrow A_{1,1}^{-1} B_1$  ▷ `trsm`
  - 3: **for**  $j = 2$  to  $J$  **do**
  - 4:  $B_j \leftarrow B_j - A_{j,j-1} Y_{j-1}$  ▷ `gemm`
  - 5:  $Y_j \leftarrow A_{j,j}^{-1} B_j$  ▷ `trsm`
  - 6: **end for**
  - 7: – *Backward substitution* –
  - 8:  $X_J \leftarrow A_{J,J}^{-\top} Y_J$  ▷ `trsm`
  - 9: **for**  $j = J - 1$  to  $1$  **do**
  - 10:  $Y_j \leftarrow Y_j - A_{j+1,j}^\top X_{j+1}$  ▷ `gemm`
  - 11:  $X_j \leftarrow A_{j,j}^{-\top} Y_j$  ▷ `trsm`
  - 12: **end for**
- 

$\mathcal{O}(Nn^2)$ . For SPD matrices, this process is numerically stable, as each Schur complement produced remains SPD, thereby ensuring that the Cholesky factorization of the diagonal blocks is always well-defined. The primary bottleneck of this approach lies in its inherent sequential nature: the computation for block  $j + 1$  relies on the results from preceding blocks. Consequently, even with a substantial number of parallel resources, the execution time scales linearly with  $N$ . Parallelism can only be leveraged within the individual block operations (e.g., `potrf`, `trsm`, `gemm`), which limits scalability for large  $N$  and underscores the need for the development of a recursive, parallel algorithm. The memory complexity is  $\mathcal{O}(Nn^2)$ , since only the  $N$  diagonal blocks of size  $n \times n$  and the  $N - 1$  off-diagonal blocks need to be stored; no global fill-in occurs beyond this block-tridiagonal pattern. In practice, the memory cost is dominated by storing these block factors together with temporary workspaces for `gemm` and `trsm` operations, but remains linear in  $N$  and quadratic in  $n$ .

**3 Parallel Recursive Algorithm** To overcome the limitations of the sequential approach, we employ a parallel recursive algorithm based on Schur complement reduction. This *divide and conquer* strategy, also known as substructuring, breaks the long sequential dependency chain, allowing the bulk of the computation to be performed in parallel using batched operations. Similarly to the sequential method, the parallel algorithm consists of two main phases: a factorization phase that computes and stores the necessary factors, and a solve phase that uses these factors to compute the solution for a given right-hand side.

**3.1 Partitioning and Reordering** The core of the recursive algorithm lies in partitioning the original block-tridiagonal system into smaller, independent sub-

systems. The key to the recursive method is to partition the  $N$  block variables into two sets: a set of  $P$  *separators* and a set of  $N - P$  *interiors*. A symmetric permutation is applied to the entire system, which rearranges the matrix, the solution matrix  $X$ , and the right-hand-side (RHS) matrix  $B$  into a  $2 \times 2$  block structure.

We illustrate this procedure with a system with  $N = 7$  and  $P = 3$ , where separators are at indices  $\{1, 4, 7\}$ . The reordered matrix is given as follows:

$$(3.1) \quad \tilde{A} = \left( \begin{array}{ccc|ccc} A_{uu} & & A_{lu} & & & \\ A_{lu}^\top & & A_{ll} & & & \\ \hline A_{2,2} & A_{3,2}^\top & 0 & 0 & A_{2,1} & 0 & 0 \\ A_{3,2} & A_{3,3} & 0 & 0 & 0 & A_{4,3}^\top & 0 \\ 0 & 0 & A_{5,5} & A_{6,5}^\top & 0 & A_{5,4} & 0 \\ 0 & 0 & A_{6,5} & A_{6,6} & 0 & 0 & A_{7,6}^\top \\ \hline A_{2,1}^\top & 0 & 0 & 0 & A_{1,1} & 0 & 0 \\ 0 & A_{4,3} & A_{5,4}^\top & 0 & 0 & A_{4,4} & 0 \\ 0 & 0 & 0 & A_{7,6} & 0 & 0 & A_{7,7} \end{array} \right)$$

The same permutation partitions the solution matrix  $X$  and RHS matrix  $B$  into components corresponding to the interiors  $(X_u, B_u)$  and separators  $(X_l, B_l)$ :

$$(3.2) \quad \tilde{X} = \begin{pmatrix} X_u \\ X_l \end{pmatrix} = \begin{pmatrix} X_2 \\ X_3 \\ X_5 \\ X_6 \\ \hline X_1 \\ X_4 \\ X_7 \end{pmatrix}, \quad \tilde{B} = \begin{pmatrix} B_u \\ B_l \end{pmatrix} = \begin{pmatrix} B_2 \\ B_3 \\ B_5 \\ B_6 \\ \hline B_1 \\ B_4 \\ B_7 \end{pmatrix}$$

The reordered system  $\tilde{A}\tilde{X} = \tilde{B}$  can now be written as a coupled  $2 \times 2$  block system of equations:

$$(3.3a) \quad A_{uu}X_u + A_{lu}X_l = B_u$$

$$(3.3b) \quad A_{lu}^\top X_u + A_{ll}X_l = B_l$$

The blocks of this reordered system can be interpreted as follows:

- $A_{uu}$  is block-diagonal, where each diagonal block  $A_{uu}^{(k)}$  corresponding to the  $k$ -th independent interior segment defined by the chosen separators. The index  $k = 1, \dots, P - 1$  enumerates these disjoint segments, each of which forms a smaller block-tridiagonal system.
- $A_{ll}$  contains the original diagonal blocks of the separators.
- $A_{lu}$  is the block-structured coupling matrix containing the original off-diagonal blocks that connect interiors to separators, where  $A_{lu}^{(k)}$  is the coupling matrix corresponding to  $A_{uu}^{(k)}$ .

This partitioned system is the foundation of our entire method. From (3.3a), we can express the interior solution  $X_u$  in terms of the unknown separator solution  $X_l$ :  $X_u = A_{uu}^{-1}(B_u - A_{lu}X_l)$ . Substituting this into (3.3b) eliminates  $X_u$  and yields a smaller system involving only the separators:

$$(3.4) \quad (A_{ll} - A_{lu}^\top A_{uu}^{-1} A_{lu})X_l = B_l - A_{lu}^\top A_{uu}^{-1} B_u$$

The matrix  $S = A_{ll} - A_{lu}^\top A_{uu}^{-1} A_{lu}$  is the Schur complement of  $A_{uu}$  in  $\tilde{A}$ . Since the Schur complement of an SPD block-tridiagonal matrix is itself SPD and block-tridiagonal, the reduced system can be recursively solved using the same Cholesky-based procedure.

This partitioning leads to a two-stage solution strategy: first, form and solve the smaller Schur complement system (3.4) to find the separator solution  $X_l$ . Second, with  $X_l$  known, substitute it back to find the interior solution  $X_u$ . Since  $A_{uu}$  is block-diagonal, the solution for  $X_u$  can be performed as a large, parallel batched solve across all independent interior segments. This reformulation establishes the groundwork for the GPU implementation, and the next step is to introduce the batched kernels that make such parallelism practical.

**3.2 Core Batched Kernels** The recursive algorithm is built upon two algorithms that operate on collections of independent block-tridiagonal systems: a batched factorization and a batched block triangular solve. These kernels, detailed in Algorithms 3.1 and 3.2, are direct parallel implementations of their sequential counterparts. They form the fundamental building blocks of the entire method, used at every level of the recursion to process the decoupled sub-problems.

We use curly braces to denote a collection of independent problems that are solved in parallel. For instance,  $\{A^{(k)}\}_{k=1}^K$  refers to a batch of  $K$  block-tridiagonal matrices, and  $\{B^{(k)}\}_{k=1}^K$  the corresponding right-hand sides. An assignment such as  $\{C^{(k)}\} \leftarrow f(\{A^{(k)}, B^{(k)}\})$  indicates that the same operation  $f$  is applied independently to each pair  $(A^{(k)}, B^{(k)})$ . This compact notation matches the interface of GPU libraries like cuBLAS, where a single batched routine orchestrates parallel execution across the entire collection. When the batch index ( $k$ ) is omitted, the notation should be read as applying to all members of the batch simultaneously.

For these batched kernels to achieve high performance on a GPU, the memory layout of the data is critical. All the block matrices of  $\{A^{(k)}\}_{k=1}^K$  for the entire batch are stored contiguously in GPU global memory. An array of pointers, with each pointer referencing the start of an individual matrix, is then constructed on the device. This pointer array is one

of the inputs to the batched kernels. This array-of-pointers interface enables a single algorithm call to orchestrate the parallel execution of thousands of small, independent problems, while ensuring coalesced memory accesses that efficiently feed data to the streaming multiprocessors. On CUDA platform, for example, cuBLAS provides a suite of batched routines (e.g.,  `cublasDpotrfBatched`,  `cublasDtrsmBatched`,  `cublasDgemmBatched`, etc.) that implement these operations efficiently on NVIDIA GPUs. Similar functionality is available in ROCm for AMD GPUs.

---

**Algorithm 3.1** Batched Block-Cholesky Factorization

---

**Require:** A batch of  $K$  block-tridiagonal systems  $\{A^{(k)}\}_{k=1}^K$  each with  $J$  diagonal blocks.

- 1: – *Operations are executed in parallel across all  $K$  systems* –
- 2:  $\{A_{1,1}^{(k)}\} \leftarrow \text{cholesky}(\{A_{1,1}^{(k)}\})$  ▷ batched `potrf`
- 3: **for**  $j = 1$  to  $J - 1$  **do**
- 4:  $\{A_{j+1,j}^{(k)\top}\} \leftarrow \{(A_{j,j}^{(k)})^{-1}A_{j,j+1}^{(k)}\}$  ▷ batched `trsm`
- 5:  $\{A_{j+1,j+1}^{(k)}\} \leftarrow \{A_{j+1,j+1}^{(k)} - A_{j+1,j}^{(k)}A_{j+1,j}^{(k)\top}\}$
- 6: ▷ batched `gemm`
- 7:  $\{A_{j+1,j+1}^{(k)}\} \leftarrow \text{cholesky}(\{A_{j+1,j+1}^{(k)}\})$
- 8: ▷ batched `potrf`
- 9: **end for**

---



---

**Algorithm 3.2** Batched Block-Cholesky Solve

---

**Require:** Factorized system matrix  $\{A^{(k)}\}_{k=1}^K$ ; RHS  $\{B^{(k)}\}_{k=1}^K$

**Ensure:** Solutions  $\{X^{(k)}\}_{k=1}^K$

- 1: – *Batched Forward Substitution* –
- 2:  $\{Y_1^{(k)}\} \leftarrow \{(A_{1,1}^{(k)})^{-1}B_1^{(k)}\}$  ▷ batched `trsm`
- 3: **for**  $j = 2$  to  $J$  **do**
- 4:  $\{\hat{B}_j^{(k)}\} \leftarrow \{B_j^{(k)} - A_{j,j-1}^{(k)}Y_{j-1}^{(k)}\}$  ▷ batched `gemm`
- 5:  $\{Y_j^{(k)}\} \leftarrow \{(A_{j,j}^{(k)})^{-1}\hat{B}_j^{(k)}\}$  ▷ batched `trsm`
- 6: **end for**
- 7: – *Batched Backward Substitution* –
- 8:  $\{X_J^{(k)}\} \leftarrow \{(A_{J,J}^{(k)})^{-\top}Y_J^{(k)}\}$  ▷ batched `trsm`
- 9: **for**  $j = J - 1$  to  $1$  **do**
- 10:  $\{\hat{Y}_j^{(k)}\} \leftarrow \{Y_j^{(k)} - A_{j+1,j}^{(k)\top}X_{j+1}^{(k)}\}$  ▷ batched `gemm`
- 11:  $\{X_j^{(k)}\} \leftarrow \{(A_{j,j}^{(k)})^{-\top}\hat{Y}_j^{(k)}\}$  ▷ batched `trsm`
- 12: **end for**

---

One can observe that each line of Algorithms 3.1 and 3.2 corresponds directly to a line in the sequential algorithms from Algorithms 2.1 and 2.2, with the key difference being that all operations are performed in parallel across the entire batch of  $K$  systems. The performance advantage of this approach comes from two main sources. First, it **amortizes** kernel launch

overhead. The cost of launching a GPU kernel is non-trivial; for a small matrix, this overhead can be orders of magnitude larger than the actual computation time. By bundling thousands of operations into a single launch, this cost is paid only once and becomes negligible. Second, it **maximizes** arithmetic intensity, which is the ratio of floating-point operations to memory operations. Batched kernels are designed to load data for many small problems into fast on-chip memory (registers and shared memory) and perform as much computation as possible before accessing slow global memory again. This keeps the arithmetic units of the GPU busy, leading to significantly higher sustained performance compared to launching one kernel per block. These batched kernels provide the fundamental building blocks of the solver. With them in place, we can now describe how the recursive algorithm assembles these kernels into a hierarchy of factorization steps.

**3.3 Recursive Factorization** The factorization phase recursively computes all factors required for the solve. This process does not form a  $LL^\top$  factorization of the full matrix in a single pass. Instead, it computes and stores the factors for each independent interior block  $A_{uu}^{(k)}$  and for the Schur complement  $S$  at each level of the hierarchy. Each level involves three main computational stages:

1. **Factorization of Interior Blocks.** The first and most computationally intensive stage is the factorization of all independent interior blocks contained within the block-diagonal matrix  $A_{uu}$ . Because all  $P - 1$  of these systems are completely decoupled from one another, this step is parallel for batched computation. It is accomplished with a single call to the batched factorization routine (Algorithm 3.1), which executes the elimination procedure for all segments simultaneously. The resulting factors for each  $A_{uu}^{(k)}$  are stored for use in the subsequent steps.
2. **Computation of the Intermediate Factors.** The Schur complement formula,  $S = A_{ll} - A_{lu}^\top A_{uu}^{-1} A_{lu}$ , requires the term  $A_{uu}^{-1} A_{lu}$ . This is computed efficiently by solving the batched linear system  $A_{uu} F = A_{lu}$  for the intermediate factor  $F$ . This factor can be interpreted as a transfer matrix; each of its block columns represents the response of the interior variables to a unit “force” applied to one of the separator variables. Computing it requires a full forward and backward substitution for each block column of  $A_{lu}$ , which is why the complete batched solve routine (Algorithm 3.2) is used. The resulting factor  $F$  is stored for use in both forming the Schur complement and in the final recursive solve.
3. **Schur Complement Formation.** With the factor

$F$  known, the Schur complement can be computed. This two-step process is detailed in Algorithm 3.3. First, a batched matrix multiplication computes the update term  $A_{lu}^\top F$ . The “Assemble” function in the second step performs a scatter-add operation, summing the contributions from each segment’s update term into the global separator matrix  $S$ . This is necessary because a single separator is typically connected to two different interior segments, and its entry in the Schur complement receives updates from both.

---

**Algorithm 3.3** Schur Complement Computation

---

**Require:** Separator matrix  $A_{ll}$ ; Coupling matrices  $A_{lu}$ ; Factors  $F$  where  $\{F^{(k)}\}_{k=1}^K = \{(A_{uu}^{(k)})^{-1}A_{lu}^{(k)}\}_{k=1}^K$ .  
**Ensure:** Schur complement matrix  $S$

- 1:  $\{\hat{S}^{(k)}\} \leftarrow \{(A_{lu}^{(k)})^\top F^{(k)}\}$  ▷ batched `gemm`
- 2:  $S \leftarrow A_{ll} - \text{Assemble}(\{\hat{S}^{(k)}\})$

---

These three stages are orchestrated by the main recursive factorization algorithm, shown in Algorithm 3.4. It executes these steps and then calls itself on the newly formed, smaller Schur complement system, continuing until the base case is reached. We introduce a crossover parameter  $N_*$ , defined as the maximum segment length for which the sequential block-Cholesky sweep is still more efficient than introducing another level of recursion; whenever  $N \leq N_*$ , the recursion terminates and the algorithm falls back to the serial factorization.

---

**Algorithm 3.4** Complete Parallel Recursive Factorization

---

**Require:** Block-tridiagonal matrix  $A$ .  
**Ensure:** Intermediate factor  $F$ ; Factorized Schur Complement  $S$ .

- 1: **if**  $N \leq N_*$  **then**
- 2:     `SERIALFACTORIZE`( $A$ ) ▷ Algorithm 2.1
- 3:     **return**
- 4: **end if**
- 5:  $A_{uu}, A_{lu}, A_{ll} \leftarrow \text{PARTITION}(A)$
- 6: `BATCHEDFACTORIZE`( $A_{uu}$ ) ▷ Algorithm 3.1
- 7:  $F \leftarrow \text{BATCHEDSOLVE}(A_{uu}, A_{lu})$  ▷ Algorithm 3.2
- 8:  $S \leftarrow \text{COMPUTESCHUR}(A_{ll}, A_{lu}, F)$  ▷ Algorithm 3.3
- 9: `RECURSIVEFACTORIZE`( $S$ ) ▷ Recursive call

---

The computational cost of this phase is dominated by the batched operations on the finest grid. While the total number of floating-point operations remains  $\mathcal{O}(Nn^3)$ , the work is now organized into a small number of large, parallel batched operations. This structure is ideal for GPUs, as it maximizes hardware utilization and hides memory latency. Furthermore, this hi-

erarchical approach improves memory access patterns. Instead of the irregular, strided access of the sequential method, the batched kernels operate on contiguous blocks of data, allowing the GPU to leverage coalesced memory transactions and its cache hierarchy more effectively. The recursive factorization produces the hierarchy of factors needed to solve the system. Once this phase is complete, the recursion can be unwound in the complementary recursive solve.

**3.4 Recursive Solve** The solve phase unwinds the recursion, working from the separators on the coarsest level back to the interiors on the finest. It uses the pre-computed factors in a two-pass process that is analogous to a block forward and backward substitution applied across the entire hierarchy. The forward pass descends the recursion, propagating information from the fine-grid RHS to the separator systems. The backward pass ascends the recursion, using the computed separator solutions to substitute back and solve for the interior variables.

**3.4.1 Separator System Right-Hand-Side Formation** The forward pass begins by computing the modified RHS for the separator system, which is mathematically equivalent to  $\hat{B}_l = B_l - A_{lu}^\top A_{uu}^{-1} B_u$ . This is the crucial step that allows the smaller separator system to be solved independently. As detailed in Algorithm 3.5, this is achieved by reusing the intermediate factor  $F$  computed during factorization. This factor is then used to compute the update term that is subtracted from the original separator RHS,  $B_l$ .

---

**Algorithm 3.5** Separator System RHS Computation

---

**Require:** Intermediate Factor  $F$ ; Interior RHS  $B_u$ ; Separator RHS  $B_l$ .  
**Ensure:** Updated separator RHS  $\hat{B}_l$ .

- 1:  $\{b^{(k)}\} \leftarrow \{-(F^{(k)})^\top B_u^{(k)}\}$  ▷ batched `gemm`
- 2:  $\hat{B}_l \leftarrow B_l + \text{Assemble}(\{b^{(k)}\})$

---

**3.4.2 Boundary Update for Interior Solves** After the recursive call returns with the separator solution  $X_l$ , the next step is to recover the interior variables  $X_u$ . Once the updated  $\hat{B}_u$  is available, the interiors are completely decoupled and can be solved independently with the batched triangular-solve routine. This completes the solve phase for the current level of recursion.

**3.4.3 The Complete Recursive Solve** The main recursive function, shown in Algorithm 3.7, orchestrates these sub-steps. The process represents a full solve of the system, transforming the initial RHS matrix  $B$  into the final solution matrix  $X$ . The Assemble

---

**Algorithm 3.6** Boundary Update

---

**Require:** Interior RHS  $B_u$ ; Separator solution  $X_l$ ;  
Coupling matrix  $A_{lu}$ .

**Ensure:** Updated interior RHS  $\hat{B}_u$ .

1:  $\{\hat{B}_u^{(k)}\} \leftarrow \{B_u^{(k)} - A_{lu}^{(k)} X_l^{(k)}\}$   $\triangleright$  batched gemm

---

step is the reverse of partitioning; it pieces together the separately computed solution matrices for the interiors ( $X_u$ ) and separators ( $X_l$ ) into the full solution matrix  $X$  in its original order.

---

**Algorithm 3.7** Complete Parallel Recursive Solve

---

**Require:** Factored block-tridiagonal matrix  $A$  at this recursion level (with access to  $A_{uu}, A_{lu}, A_{ll}$  and stored factors); Factored Schur complement  $S$ ; Intermediate factor  $F$ ; RHS  $B$ .

**Ensure:** Solution  $X$ .

1: **if**  $N \leq N_*$  **then**  
2:  $X \leftarrow \text{SERIALSOLVE}(A, B)$   $\triangleright$  Algorithm 2.2  
3: **return**  $X$ .  
4: **end if**  
5:  $B_u, B_l \leftarrow \text{PARTITION}(B)$   
6:  $\hat{B}_l \leftarrow \text{COMPUTESeparatorRHS}(F, B_u, B_l)$   
7:  $\triangleright$  Algorithm 3.5  
8:  $X_l \leftarrow \text{RECURSIVESOLVE}(S, \hat{B}_l)$   $\triangleright$  Recursive call  
9:  $\hat{B}_u \leftarrow \text{UPDATEBOUNDARY}(B_u, X_l, F)$   
10:  $\triangleright$  Algorithm 3.6  
11:  $X_u \leftarrow \text{BATCHEDSOLVE}(A_{uu}, \hat{B}_u)$   $\triangleright$  Algorithm 3.2  
12:  $X \leftarrow \text{ASSEMBLE}(X_u, X_l)$   
13: **return**  $X$ .

---

The hierarchical data flow ensures that communication and dependencies are localized. The forward pass propagates information from the fine-grid RHS matrices to the separator system. After the recursive call solves for the “keystone” separator variables ( $X_l$ ), the backward pass uses this solution to obtain the remaining interior variables ( $X_u$ ). Like the factorization, each step is composed of large, batched operations, maintaining high GPU occupancy and ensuring high efficiency.

**4 Experiments** We evaluate the performance of our proposed solver, **TBD-GPU**, on large synthetic block-tridiagonal systems. We benchmark against NVIDIA’s GPU sparse Cholesky solver (cuDSS), AMD and NVIDIA baselines using batched and sequential block solvers, and three CPU solvers (CHOLMOD, MA57, and LDLFactorizations.jl). Experiments are conducted in double precision (FP64).

**4.1 Experimental Setup** All CPU experiments were run on an Intel Xeon Platinum 8562Y+ system with 1007 GB of RAM, using Intel MKL for dense ker-

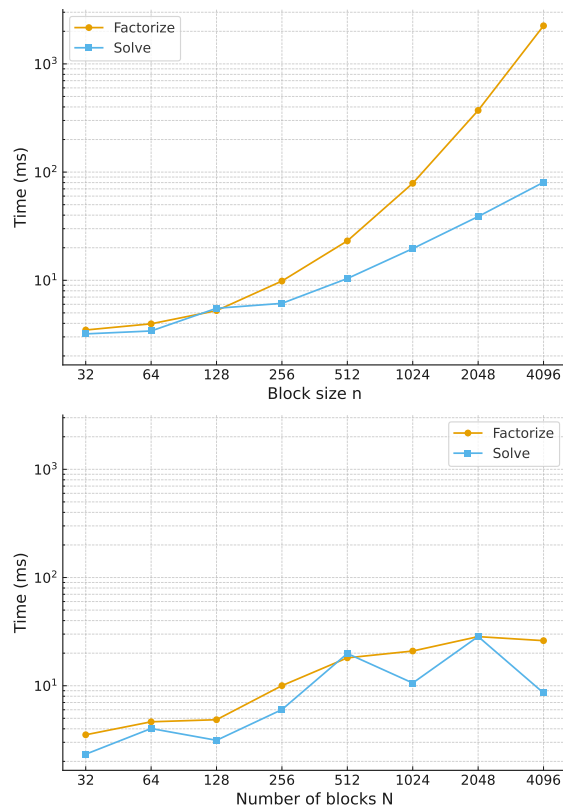


Figure 4.1: Scaling performance of GPU batched solver. Top: factorize and solve times vs. block size  $n$  (fixed  $N = 64$ ). Bottom: factorize and solve times vs. number of blocks  $N$  (fixed  $n = 64$ ).

nels. GPU experiments were conducted on an NVIDIA H200 (141 GB HBM3e, CUDA 12.4) and an AMD MI300X (128 GB HBM3e, ROCm 6.4.1). We measure time-to-solution as the primary performance metric, decomposed into factorization and solve phases. Accuracy is reported via the Euclidian norm of the residual  $\|Ax - b\|_2$ . Each reported result is the mean over 10 runs.

*Synthetic SPD block-tridiagonal generation.* All benchmark problems in this work are based on randomly generated SPD block-tridiagonal matrices. The construction ensures that the matrices respect the block structure assumed by the solver while remaining well-conditioned and reproducible across runs.

We benchmark across fixed total problem size  $N \times n = 262,144$ , sweeping  $n \in \{32, 64, 128, 256, 512, 1024\}$  (and corresponding  $N$ ). Table 4.1 summarizes performance in FP64. Figure 4.1 shows scaling results for the GPU batched solver. The top panel varies the block size  $n$  at fixed number of blocks  $N = 64$ , while the bottom

Table 4.1: FP64 sweep for  $N \times n = 262144$ ,  $n \in \{32, 64, 128, 256, 512, 1024\}$ . Metrics: Factorization, Solve, Total (F+S), Residual  $\|Ax - b\|_2$ . Values are the mean of 10 runs.

$N$	$n$	Metric	GPU					CPU		
			cuDSS (NVIDIA)	Batched (NVIDIA)	Seq (NVIDIA)	Batched (AMD)	Seq (AMD)	MA57	CHOLMOD	LDL <sup>T</sup>
256	1024	Factorization	298.02	<b>273.35</b>	391.91	356.50	841.33	104289.74	59434.58	247792.31
		Solve	48.57	<b>41.71</b>	224.02	113.55	212.11	658.92	428.91	1977.38
		Total	346.59	<b>315.06</b>	615.94	470.05	1053.44	104948.67	59863.49	249769.69
		Residual	8.48e-10	7.60e-10	1.20e-09	6.35e-10	<b>6.34e-10</b>	1.71e-09	1.42e-09	2.11e-09
512	512	Factorization	259.35	<b>120.56</b>	364.10	225.54	824.68	35962.12	25748.44	69248.17
		Solve	55.36	<b>41.53</b>	246.74	130.63	345.23	330.25	222.63	1023.62
		Total	314.71	<b>162.09</b>	610.84	356.17	1169.91	36292.36	25971.07	70271.79
		Residual	3.13e-10	2.99e-10	4.20e-10	<b>2.24e-10</b>	2.25e-10	5.87e-10	2.96e-10	7.29e-10
1024	256	Factorization	173.87	<b>61.72</b>	405.98	224.81	873.97	13619.00	11085.06	15969.64
		Solve	<b>6.29</b>	21.70	352.26	24.23	430.72	172.14	116.98	515.54
		Total	180.16	<b>83.42</b>	758.24	249.04	1304.69	13791.14	11202.04	16485.17
		Residual	1.17e-10	<b>1.02e-10</b>	1.53e-10	<b>1.02e-10</b>	1.03e-10	1.15e-10	1.07e-10	2.59e-10
2048	128	Factorization	<b>29.87</b>	41.91	517.58	245.73	1080.20	5923.22	5127.79	4385.00
		Solve	<b>2.53</b>	30.86	566.19	42.36	721.62	94.93	72.29	285.93
		Total	<b>32.40</b>	72.77	1083.78	288.09	1801.83	6018.14	5200.08	4670.93
		Residual	4.22e-11	<b>3.95e-11</b>	5.53e-11	4.66e-11	4.65e-11	4.22e-11	4.03e-11	9.17e-11
4096	64	Factorization	<b>10.66</b>	12.65	737.65	11.93	1016.87	2267.96	2031.70	1117.63
		Solve	<b>1.13</b>	6.84	953.29	12.00	1271.82	42.78	34.71	111.78
		Total	<b>11.79</b>	19.49	1690.94	23.93	2288.69	2310.75	2066.41	1229.41
		Residual	<b>1.57e-11</b>	<b>1.57e-11</b>	2.09e-11	1.97e-11	1.98e-11	2.80e-11	2.33e-11	3.36e-11
8192	32	Factorization	<b>4.33</b>	7.95	1213.97	6.49	1618.96	1037.27	1069.48	357.45
		Solve	<b>0.68</b>	4.36	1779.63	13.20	2549.24	26.61	21.12	55.06
		Total	<b>5.01</b>	12.32	2993.60	19.69	4168.20	1063.87	1090.60	412.50
		Residual	<b>6.05e-12</b>	6.41e-12	8.14e-12	7.52e-12	7.48e-12	1.05e-11	8.56e-12	1.19e-11

panel varies the number of blocks  $N$  at fixed block size  $n = 64$ . Our code is available in the link specified in the previous footnote.

## 4.2 Discussion of Results

*GPU vs. CPU baselines.* Across all problem sizes, GPU-based solvers outperform CPU solvers by one to three orders of magnitude in time-to-solution. CPU solvers remain competitive only at very small block sizes ( $n \leq 64$ ), but quickly become impractical for larger  $n$ , with factorization times in the tens of seconds even for moderately sized problems. These comparisons confirm that GPUs are the correct hardware target for block-tridiagonal systems at scale.

*TBD-GPU vs. cuDSS.* The most relevant comparison is against the sparse Cholesky solver of NVIDIA cuDSS. On small to moderate block sizes ( $n \leq 128$ ), cuDSS achieves extremely low runtimes by leveraging optimized sparse kernels. However, as  $n$  increases, **TBD-GPU** consistently outperforms cuDSS. For instance, at  $(N, n) = (1024, 256)$  in FP64, **TBD-GPU** achieves 83 ms compared to 180 ms for cuDSS. At  $(4096, 64)$ , **TBD-GPU** remains within a factor of two of cuDSS. The advantage of **TBD-GPU** becomes most

pronounced for large blocks ( $n \geq 512$ ), where its batched dense-kernel approach fully exploits GPU memory bandwidth and tensor cores.

*AMD vs. NVIDIA performance.* On AMD MI300X GPUs, our solver achieves performance close to that on NVIDIA H200. Nonetheless, the same scaling behavior is observed: batched TBD-GPU consistently outperforms sequential GPU solvers and approaches the efficiency of cuDSS on small problems, while overtaking it at larger  $n$ . This suggests that the algorithm is portable across architectures and primarily limited by backend library maturity rather than hardware.

*Scaling behavior.* In Figure 4.1, with  $N$  fixed, the total work per step follows dense block costs (factorization  $\Theta(n^3)$  and solves  $\Theta(n^2)$ ) and the wall-time curves grow accordingly, with factorization dominant. With  $n$  fixed, the total work increases proportionally to  $N$ , but the wall time grows sublinearly due to the multilevel recursive algorithm.

*Overall trends.* The results show a clear regime split. For *small blocks*, cuDSS remains highly competitive due to specialized sparse triangular kernels. For *large blocks*, **TBD-GPU** overtakes cuDSS by fully exploiting block structure, reaching up to  $3\times$  speedups in

factorization and  $2\times$  in total time. Compared to CPU solvers, both GPU methods provide one to two orders of magnitude acceleration.

### 4.3 Application: Kalman Smoothing

Kalman smoothing arises in problems where we wish to estimate the trajectory of a hidden state from noisy measurements. Typical applications include navigation, tracking and signal processing, where the underlying dynamics are approximately linear and the uncertainties are modeled as Gaussian noise.

The system evolves according to

$$(4.1) \quad x_k = G_k x_{k-1} + w_k, \quad k = 1, \dots, N,$$

$$(4.2) \quad z_k = H_k x_k + v_k, \quad k = 1, \dots, N,$$

where  $x_k \in \mathbb{R}^n$  is the hidden state at time  $k$ ,  $z_k \in \mathbb{R}^m$  is the noisy measurement,  $G_k \in \mathbb{R}^{n \times n}$  is the state transition matrix, and  $H_k \in \mathbb{R}^{m \times n}$  is the observation matrix. The process and measurement noises,  $w_k \sim \mathcal{N}(0, Q_k)$  and  $v_k \sim \mathcal{N}(0, R_k)$ , are independent with known covariances. The initial condition  $x_0$  is assumed known, with  $G_1 = I_n$ .

Estimating the most likely sequence of states given all measurements is known as the maximum a posteriori (MAP) smoothing problem. This is equivalent to minimizing the negative log-posterior,

$$(4.3) \quad \min_{x_1, \dots, x_N} \sum_{k=1}^N \frac{1}{2} \|z_k - H_k x_k\|_{R_k^{-1}}^2 + \sum_{k=1}^N \frac{1}{2} \|x_k - G_k x_{k-1}\|_{Q_k^{-1}}^2.$$

Stacking all states  $x^T = [x_1^T, \dots, x_N^T]$  and all measurements  $z^T = [z_1^T, \dots, z_N^T]$ , we obtain

$$\min_x \frac{1}{2} \|Hx - z\|_{R^{-1}}^2 + \frac{1}{2} \|Gx - \zeta\|_{Q^{-1}}^2,$$

where the matrices  $H$ ,  $R$ ,  $Q$ ,  $G$ , and the vector  $\zeta$  are defined as in [3]. The corresponding optimality conditions yield an SPD block-tridiagonal system:

$$(4.4) \quad (H^T R^{-1} H + G^T Q^{-1} G) x = H^T R^{-1} z + G^T Q^{-1} \zeta.$$

The system can be written compactly as  $Ax = b$ , where the coefficient matrix in (4.4) has  $n \times n$  blocks

$$A_{k,k} = Q_k^{-1} + G_{k+1}^T Q_{k+1}^{-1} G_{k+1} + H_k^T R_k^{-1} H_k,$$

$$A_{k+1,k} = -Q_{k+1}^{-1} G_{k+1},$$

with the convention  $G_{N+1} = 0$ , and the right-hand side blocks are  $b_k = H_k^T R_k^{-1} z_k + G_k^T Q_k^{-1} \zeta_k$ . This matches exactly the block-tridiagonal structure targeted by our recursive GPU solver. Classical smoothers such as Rauch–Tung–Striebel (RTS), Mayne (M), and Mayne–Fraser (MF) can be interpreted as specific block

elimination schemes for (4.4). Here we emphasize that Kalman smoothing ultimately reduces to solving an SPD block-tridiagonal system, making it a natural application for our method.

*Neuroscience experiment.* To showcase the solver in a realistic high-dimensional regime, we draw inspiration from neural population dynamics in motor cortex, where latent activity exhibits smooth rotational structure and is observed through a large number of noisy spike trains [22, 7]. We instantiate the model with latent state dimension  $n = 256$ , observation dimension  $m = 1024$ , and horizon  $N = 100$  (10 s sampled at  $\Delta t = 0.1$  s).

The latent dynamics are modeled by constructing  $G$  from damped two-dimensional rotations. The observation matrix  $H$  is tall and well-conditioned. The process noise covariance  $Q$  is dense and symmetric positive definite, while the observation noise covariance  $R$  is diagonal and scaled larger than  $Q$  to reflect more reliable latent dynamics than sensor observations.

*Evaluation.* We report (i) the residual norm  $\|Ax - b\|_2$  and (ii) solver wall-clock times for initialization, factorization, and solution phases. Both **TBD-GPU** and cuDSS converge to the same residual level of  $\sim 6 \times 10^{-12}$ , confirming numerical equivalence. The measured times (in milliseconds) are as follows:

Solver	Init	Factor	Solve	Total
<b>TBD-GPU</b>	109.6	13.3	8.6	21.9
cuDSS	246.5	27.5	1.8	29.3

On this tall-observation, large-state problem, **TBD-GPU** avoids general sparse overhead and achieves a clear runtime advantage over cuDSS. We include figures about the recovered latent trajectory in Appendix A.

**5 Conclusions** We have presented the **TBD-GPU** solver, a GPU implementation for large-scale block-tridiagonal linear systems. By combining a recursive Schur complement strategy with batched dense linear algebra kernels, our approach overcomes the inherent sequential bottlenecks of traditional algorithms while maximizing GPU utilization. On synthetic block-tridiagonal problems, **TBD-GPU** consistently outperforms sequential GPU solvers while remaining competitive compared to NVIDIA’s cuDSS on large block sizes. The structure-aware design of **TBD-GPU** allows it to exploit BLAS and LAPACK batched kernels more effectively than general-purpose sparse solvers. However, since **TBD-GPU** relies on sequential calls to batched routines at each recursion level, it requires sufficiently large block sizes to amortize kernel launch overheads. In the future, we plan to develop a solver that fully fuses the recursive algorithm into a single GPU kernel,

to minimize the kernel launch overhead and further improve performance on smaller block sizes.

**Acknowledgement** We gratefully acknowledge generous funding provided by Charles Cahn. We also thank Ryan Senne for valuable discussions on the neuroscience applications of this work.

## References

- [1] ADVANCED MICRO DEVICES, INC., *ROCm documentation*. <https://rocm.docs.amd.com/>, 2025.
- [2] X. AI, G. MANIA, H. M. GRAY, M. KUHN, AND N. STYLES, *A gpu-based kalman filter for track fitting*, Computing and Software for Big Science, 5 (2021), p. 20, <https://doi.org/10.1007/s41781-021-00065-z>, <https://doi.org/10.1007/s41781-021-00065-z>.
- [3] A. Y. ARAVKIN, J. V. BURKE, B. M. BELL, AND G. PILLONETTO, *Algorithms for block tridiagonal systems: Stability results for generalized kalman smoothing*, IFAC-PapersOnLine, 54 (2021), pp. 821–826, <https://doi.org/https://doi.org/10.1016/j.ifacol.2021.08.463>, <https://www.sciencedirect.com/science/article/pii/S2405896321012386>. 19th IFAC Symposium on System Identification SYSID 2021.
- [4] A. Y. ARAVKIN, J. V. BURKE, AND G. PILLONETTO, *Optimization Viewpoint on Kalman Smoothing with Applications to Robust and Sparse Estimation*, Springer Berlin Heidelberg, Berlin, Heidelberg, 2014, pp. 237–280, [https://doi.org/10.1007/978-3-642-38398-4\\_8](https://doi.org/10.1007/978-3-642-38398-4_8), [https://doi.org/10.1007/978-3-642-38398-4\\_8](https://doi.org/10.1007/978-3-642-38398-4_8).
- [5] P. A. BELOV, E. R. NUGUMANOV, AND S. L. YAKOVLEV, *The arrowhead decomposition method for a block-tridiagonal system of linear equations*, Journal of Physics: Conference Series, 929 (2017), p. 012035, <https://doi.org/10.1088/1742-6596/929/1/012035>, <https://dx.doi.org/10.1088/1742-6596/929/1/012035>.
- [6] J. BEZANSON, A. EDELMAN, S. KARPINSKI, AND V. B. SHAH, *Julia: A fresh approach to numerical computing*, SIAM Review, 59 (2017), pp. 65–98, <https://doi.org/10.1137/141000671>, <https://doi.org/10.1137/141000671>.
- [7] M. M. CHURCHLAND, J. P. CUNNINGHAM, M. T. KAUFMAN, J. D. FOSTER, P. NUYUJUKIAN, S. I. RYU, AND K. V. SHENOY, *Neural population dynamics during reaching*, Nature, 487 (2012), pp. 51–56, <https://doi.org/10.1038/nature11129>, <https://doi.org/10.1038/nature11129>.
- [8] J. DONGARRA, S. HAMMARLING, N. HIGHAM, S. RELTON, AND M. ZOUNON, *Optimized batched linear algebra for modern architectures*, in Euro-Par 2017, F. Rivera, T. Pena, and J. Cabaleiro, eds., Lecture Notes in Computer Science (including subseries Lecture Notes in Artificial Intelligence and Lecture Notes in Bioinformatics), Springer Verlag, 2017, pp. 511–522, [https://doi.org/10.1007/978-3-319-64203-1\\_37](https://doi.org/10.1007/978-3-319-64203-1_37). Publisher Copyright: © 2017, Springer International Publishing AG.; 23rd International Conference on Parallel and Distributed Computing, Euro-Par 2017 ; Conference date: 28-08-2017 Through 01-09-2017.
- [9] A. DU, E. ADABAG, G. BRAVO, AND B. PLANCHER, *Gato: Gpu-accelerated and batched trajectory optimization for scalable edge model predictive control*, 2025, <https://arxiv.org/abs/2510.07625>, <https://arxiv.org/abs/2510.07625>.
- [10] W. GANDER AND G. H. GOLUB, *Cyclic reduction – history and applications*, in Proceedings of the Workshop on Scientific Computing, Springer-Verlag, 1997, <https://people.inf.ethz.ch/gander/papers/cyclic.pdf>.
- [11] R. W. HOCKNEY, *A fast direct solution of poisson’s equation using fourier analysis*, J. ACM, 12 (1965), p. 95–113, <https://doi.org/10.1145/321250.321259>, <https://doi.org/10.1145/321250.321259>.
- [12] K.-H. KIM, J.-H. KANG, X. PAN, AND J.-I. CHOI, *Pascal.tdma: A library of parallel and scalable solvers for massive tridiagonal system*, Computer Physics Communications, 260 (2021), p. 107722, <https://doi.org/https://doi.org/10.1016/j.cpc.2020.107722>.
- [13] C. KLEIN AND R. STRZODKA, *Tridigpu: A gpu library for block tridiagonal and banded linear equation systems*, ACM Trans. Parallel Comput., 10 (2023), <https://doi.org/10.1145/3580373>, <https://doi.org/10.1145/3580373>.
- [14] J. NOCEDAL AND S. WRIGHT, *Numerical optimization*, Springer series in operations research and financial engineering, Springer, New York, NY, 2. ed. ed., 2006, [http://gso.gbv.de/DB=2.1/CMD?ACT=SRCHA&SRT=YOP&IKT=1016&TRM=ppn+502988711&sourceid=fbw\\_bibsonomy](http://gso.gbv.de/DB=2.1/CMD?ACT=SRCHA&SRT=YOP&IKT=1016&TRM=ppn+502988711&sourceid=fbw_bibsonomy).
- [15] NVIDIA CORPORATION, *cublas library user guide*. <https://docs.nvidia.com/cuda/cublas/>, 2025.
- [16] NVIDIA CORPORATION, *cusolver library user guide*. <https://docs.nvidia.com/cuda/cusolver/>, 2025.
- [17] NVIDIA CORPORATION, *cusolver library*. <https://docs.nvidia.com/cuda/cusolver/>, 2025.
- [18] NVIDIA CORPORATION, *cusparse library user guide*. <https://docs.nvidia.com/cuda/cusparse/>, 2025.
- [19] F. PACAUD AND S. SHIN, *GPU-accelerated dynamic nonlinear optimization with ExaModels and MadNLP*, in 2024 IEEE 63rd Conference on Decision and Control (CDC), dec 2024, pp. 5963–5968, <https://doi.org/10.1109/CDC56724.2024.10886720>.
- [20] H. E. RAUCH, F. TUNG, AND C. T. STRIEBEL, *Maximum likelihood estimates of linear dynamic systems*, AIAA Journal, 3 (1965), pp. 1445–1450, <https://doi.org/10.2514/3.3166>.
- [21] S. C. RENNICH, D. STOSIC, AND T. A. DAVIS, *Accelerating Sparse Cholesky Factorization on GPUs*, in 2014 4th Workshop on Irregular Applications: Architectures and Algorithms (IA<sup>3</sup>), nov 2014, pp. 9–16, <https://doi.org/10.1109/IA335182.2014.10612387>.
- [22] D. A. SABATINI AND M. T. KAUFMAN, *Reach-dependent reorientation of rotational dynamics in motor cortex*, Nature Communications, 15 (2024), p. 7007, <https://doi.org/10.1038/s41467-024-51308-7>, <https://doi.org/10.1038/s41467-024-51308-7>.
- [23] B. F. SMITH, P. E. BJØRSTAD, AND W. D. GROPP, *Domain decomposition: parallel multilevel methods for elliptic partial differential equations*, Cambridge University Press, USA, 1996.

- [24] R. A. SWEET, *A cyclic reduction algorithm for solving block tridiagonal systems of arbitrary dimension*, SIAM Journal on Numerical Analysis, 14 (1977), pp. 706–720, <https://doi.org/10.1137/0714048>, <https://doi.org/10.1137/0714048>.
- [25] A. V. TEREKHOV, *A fast parallel algorithm for solving block-tridiagonal systems of linear equations including the domain decomposition method*, Parallel Computing, 39 (2013), pp. 245–258, <https://doi.org/https://doi.org/10.1016/j.parco.2013.03.003>, <https://www.sciencedirect.com/science/article/pii/S0167819113000367>.
- [26] L. H. THOMAS, *Elliptic problems in linear differential equations over a network*, tech. report, Watson Scientific Computing Laboratory, Columbia University, 1949. Unpublished Report.
- [27] D. TOLMACHEV, P. MARTI, G. CASTIGLIONI, AND A. JACKSON, *High performance solution of tridiagonal systems on the gpu*, ACM Trans. Parallel Comput., 12 (2025), <https://doi.org/10.1145/3716171>, <https://doi.org/10.1145/3716171>.
- [28] S. TOMOV, J. DONGARRA, M. BABOULIN, J. KURZAK, R. C. WHALEY, H. LTAIEF, AND P. LUSZCZEK, *MAGMA: A new generation of linear algebra libraries for heterogeneous architectures*, in Heterogeneity in Computing Workshop (HCW 2010), 2010. Held in conjunction with IPDPS 2010.
- [29] S. J. WRIGHT, *Partitioned Dynamic Programming for Optimal Control*, SIAM Journal on Optimization, 1 (1991), pp. 620–642, <https://doi.org/10.1137/0801037>.

### A Kalman Smoothing Plots

*Discussion.* This example highlights the qualitative behavior of our smoother on a high-dimensional latent system. Figure A.1 illustrates the recovered latent trajectory: the smoothed estimates (dashed) closely track the true latent dynamics (solid) across two representative coordinates in the rotational subspace, confirming phase and amplitude alignment.

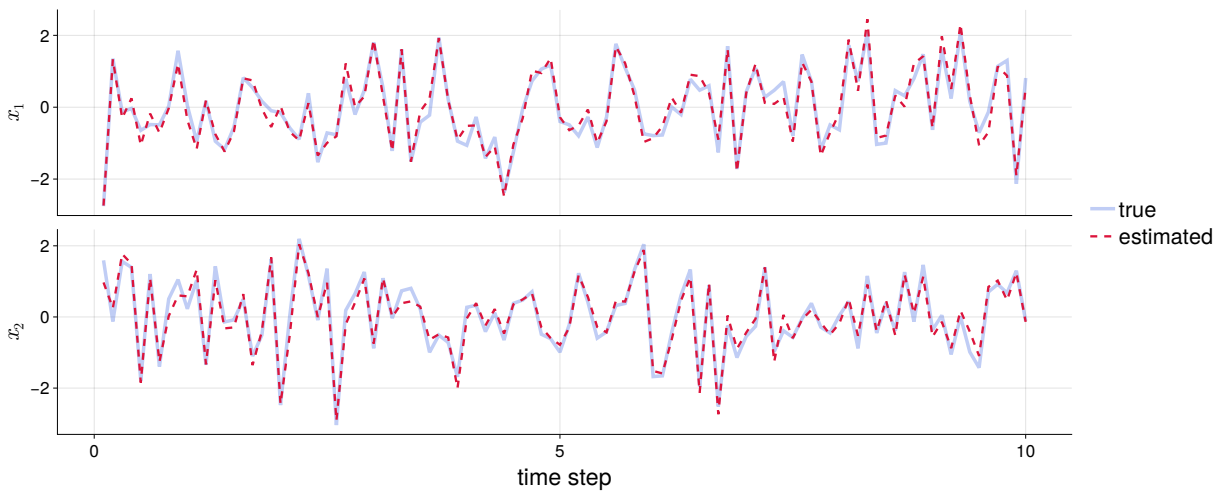


Figure A.1: Kalman smoothing with rotational latent dynamics ( $n=256$ ,  $m=1024$ ,  $N=100$ ). We plot the ground truth (solid) and smoothed trajectory (dash) in a representative 2D oscillatory subspace.